

A NEW BAYESIAN UNMIXING ALGORITHM FOR HYPERSPECTRAL IMAGES MITIGATING ENDMEMBER VARIABILITY

Abderrahim Halimi⁽¹⁾, Nicolas Dobigeon⁽¹⁾, Jean-Yves Tournet⁽¹⁾ and Paul Honeine⁽²⁾

⁽¹⁾ University of Toulouse, IRIT/INP-ENSEEIH/TéSA, Toulouse, France

⁽²⁾ Institut Charles Delaunay (CNRS), Université de technologie de Troyes, Troyes, France.

ABSTRACT

This paper presents an unsupervised Bayesian algorithm for hyperspectral image unmixing accounting for endmember variability. Each image pixel is modeled by a linear combination of random endmembers to take into account endmember variability in the image. The coefficients of this linear combination (referred to as abundances) allow the proportions of each material (endmembers) to be quantified in the image pixel. An additive noise is also considered in the proposed model generalizing the normal compositional model. The proposed Bayesian algorithm exploits spatial correlations between adjacent pixels of the image and provides spectral information by achieving a spectral unmixing. It estimates both the mean and the covariance matrix of each endmember in the image. A spatial classification is also obtained based on the estimated abundances. Simulations conducted with synthetic and real data show the potential of the proposed model and the unmixing performance for the analysis of hyperspectral images.

Index Terms— Hyperspectral imagery, endmember variability, image classification, Hamiltonian Monte-Carlo.

1. INTRODUCTION

Spectral unmixing (SU) consists of decomposing a pixel spectrum as a linear combination of physical materials contained in a hyperspectral (HS) image, known as *endmembers*, and of estimating the corresponding proportions or *abundances* [1]. The variations of endmember spectra along the image has been identified as one of the most profound sources of error in abundance estimation [2, 3]. This variation is referred to as *spectral endmember variability* (SEV) and is receiving a growing interest in the HS community [2, 3]. Many algorithms have been proposed in the literature to mitigate SEV effects. In particular, a class of models considers endmembers as statistical distributions [3] and thus assumes that each pixel of the image is a linear combination of random endmembers. These models include the beta compositional model

This work was supported in part by the HYPANEMA ANR Project under Grant ANR-12-BS03-003, and in part by the Thematic Trimester on Image Processing of the CIMI Labex, Toulouse, France, under Grant ANR-11-LABX-0040-CIMI within the Program ANR-11-IDEX-0002-02.

[4] and the normal compositional model (NCM) [5–7]. This paper studies a generalization of the NCM model accounting for Gaussian variability for the endmembers (as for the NCM) and an additive Gaussian noise modeling fitting errors (which was not present in the NCM). Moreover, the proposed model considers a different mean and covariance matrix for each endmember to analyze each component separately. This paper also considers spatial correlation between adjacent pixels of the image using Markov random fields (MRFs) as in [8, 9]. More precisely, the image is segmented into regions sharing similar abundance characteristics which improves the unmixing quality [8, 9]. In addition to the abundance Dirichlet priors, the proposed Bayesian model assumes appropriate prior for the remaining parameters/hyperparameters to satisfy the known physical constraints.

Since the standard Bayesian estimators (minimum mean square error (MMSE) and maximum a posteriori (MAP) estimators) associated with the proposed model are not easy to be computed in closed-form, they are approximated using samples generated by a Markov chain Monte Carlo (MCMC) algorithm and asymptotically distributed according to the posterior of interest. This generation is performed by a Gibbs sampler coupled with a constrained Hamiltonian Monte Carlo (CHMC) method that has been introduced in [10, Chap. 5] and applied for HS-SU in [11].

The paper is structured as follows. The proposed mixing and hierarchical Bayesian models accounting for SEV in HS images are introduced in Section 2. Section 3 analyzes the performance of the proposed algorithm when applied to synthetic images. Results on real HS images are presented in Section 4 whereas conclusions and future works are reported in Section 5.

2. HIERARCHICAL BAYESIAN MODEL

2.1. Mixing model

Let N be the number of pixels of the observed HS image. Each pixel \mathbf{y}_n , of size $(L \times 1)$, is observed in L spectral bands. The classical LMM assumes that the pixel spectrum \mathbf{y}_n is a linear combination of R deterministic endmembers \mathbf{s}_r , $r \in \{1, \dots, R\}$, corrupted by an additive independent and identically distributed (iid) noise e_n as follows

$$\mathbf{y}_n = \sum_{r=1}^R a_{rn} \mathbf{s}_r + \mathbf{e}_n \quad (1)$$

with $\mathbf{e}_n \sim \mathcal{N}(\mathbf{0}_L, \psi_n^2 \mathbf{I}_L)$, $\psi_n \in \mathbb{R}$, $\mathbf{0}_L$ is an $(L \times 1)$ vector of 0, \mathbf{I}_L is the $(L \times L)$ identity matrix and $\mathbf{a}_n = [a_{1n}, \dots, a_{Rn}]^T$ is the $(R \times 1)$ abundance vector of the n th pixel.

As previously mentioned, the endmembers generally vary from one pixel to another of the observed image [3]. In this paper, we introduce a model taking into account this variability. The proposed model can be seen as a generalization of the NCM model (GNCM) since it introduces an additional residual Gaussian noise \mathbf{e} as follows

$$\mathbf{y}_n = \sum_{r=1}^R a_{rn} \mathbf{s}_{rn} + \mathbf{e}_n = \mathbf{S}_n \mathbf{a}_n + \mathbf{e}_n \quad (2)$$

where $\mathbf{s}_{rn} \sim \mathcal{N}(\mathbf{m}_r, \text{diag}(\boldsymbol{\sigma}_r^2))$, $\mathbf{S}_n = [\mathbf{s}_{1n}, \dots, \mathbf{s}_{Rn}]$, $\boldsymbol{\sigma}_r^2 = [\sigma_{r1}^2, \dots, \sigma_{rL}^2]$ is the variance vector of the r th endmember and $\mathbf{M} = [\mathbf{m}_1, \dots, \mathbf{m}_R]$ is the $(L \times R)$ matrix containing the endmember means of the image (and where a_{rn} and \mathbf{e}_n are defined as in (1)). The main difference between the proposed GNCM (2) and the LMM is that the endmember matrix \mathbf{S}_n depends on each observed pixel in order to account for the SEV. Each pure material is then represented in a given pixel by an endmember \mathbf{s}_{rn} that has its own Gaussian distribution whose variances $\boldsymbol{\sigma}_r^2$ change from one band to another. This allows the GNCM to capture the spectral variations of each physical element with respect to each spectral band. The additional Gaussian noise \mathbf{e}_n makes the proposed model more robust with respect to mismodeling. Note finally that the proposed model reduces to the NCM for $\psi_n^2 = 0$, $\forall n$. Thus, it generalizes the model of [6, 7] by considering a non-isotropic covariance matrix for each endmember. Finally, for both LMM and GNCM, the abundance vector \mathbf{a}_n contains proportions and thus should satisfy the physical positivity and sum-to-one (PSTO) constraints $a_{rn} \geq 0, \forall r \in \{1, \dots, R\}$ and $\sum_{r=1}^R a_{rn} = 1$.

2.2. Likelihood

Using the observation model (2), the Gaussian properties of both the noise sequence \mathbf{e}_n and the endmembers, and exploiting independence between the noise samples in different spectral bands, yield

$$f(\mathbf{y}_n | \mathbf{A}, \mathbf{M}, \boldsymbol{\Sigma}, \boldsymbol{\Psi}) \propto \left(\frac{1}{\prod_{l=1}^L \Omega_{ln}} \right)^{\frac{1}{2}} \times \exp \left\{ -\frac{1}{2} \boldsymbol{\Lambda}_{:n}^T [(\mathbf{y}_n - \mathbf{M} \mathbf{a}_n) \odot (\mathbf{y}_n - \mathbf{M} \mathbf{a}_n)] \right\} \quad (3)$$

where $\boldsymbol{\Omega} = \boldsymbol{\Sigma}^T (\mathbf{A} \odot \mathbf{A}) + \mathbf{K}$ is an $(L \times N)$ matrix, $\boldsymbol{\Sigma}$ is an $(R \times L)$ matrix gathering the endmember variances (with $\boldsymbol{\Sigma}_{r,l} = \sigma_{rl}^2$), $\mathbf{K} = \mathbf{1}_L \otimes \boldsymbol{\Psi}$ is an $(L \times N)$ matrix whose rows are equal to $\boldsymbol{\Psi} = [\psi_1^2, \dots, \psi_n^2]$, $\mathbf{1}_L$ is an $(L \times 1)$ vector of 1, $\boldsymbol{\Lambda}$ is an $(L \times N)$ matrix with $\Lambda_{ln} = \frac{1}{\Omega_{ln}}$, \odot denotes the Hadamard (termwise) product and \otimes denotes the

Kronecker product. Moreover, contrary to the LMM, Eq. (3) shows that the elements¹ of $\boldsymbol{\Omega}$ depend jointly on the pixel abundances and on the pixel index $\#n$. This property was also satisfied by the NCM model as previously shown in [6,7]. Note finally that by assuming independence between the observed pixels, the joint likelihood of the observation matrix $f(\mathbf{Y} | \mathbf{A}, \mathbf{M}, \boldsymbol{\Sigma}, \boldsymbol{\Psi})$ can be expressed as the product of N likelihoods as defined in (3).

2.3. Parameter/hyperparameter priors

This section introduces the prior distributions chosen for the parameters of the proposed GNCM model. The unknown parameters of this model include the endmember mean matrix \mathbf{M} , the $(R \times L)$ matrix $\boldsymbol{\Sigma}$, the $(R \times N)$ abundance matrix $\mathbf{A} = [\mathbf{a}_1, \dots, \mathbf{a}_N]$, the $(1 \times N)$ label vector \mathbf{z} and the $(1 \times N)$ vector $\boldsymbol{\Psi}$ containing the noise variances.

2.3.1. Label prior

This paper proposes to consider the spatial correlations between adjacent image pixels by dividing the observed image into K classes sharing the same abundance properties [9]. Each pixel is assigned to a specific class by using a latent label variable z_n . A Markov random field prior is then assigned for z_n as follows $f(z_n | \mathbf{z}_{\setminus n}) = f(z_n | \mathbf{z}_{\nu(n)})$, where $\nu(n)$ denotes the pixel neighborhood (a four neighborhood structure will be considered in this paper), $\mathbf{z}_{\nu(n)} = \{z_i, i \in \nu(n)\}$ and $\mathbf{z}_{\setminus n} = \{z_i, i \neq n\}$. As in [8, 9, 12], this paper considers a Potts-Markov model which is appropriate for HS image segmentation. The prior of \mathbf{z} is obtained using the Hammersley-Clifford theorem, $f(\mathbf{z}) = \frac{1}{G(\beta)} \exp \left[\beta \sum_{n=1}^N \sum_{n' \in \nu(n)} \delta(z_n - z_{n'}) \right]$, where $\beta > 0$ is the granularity coefficient, $G(\beta)$ is a normalizing (or partition) constant and $\delta(\cdot)$ is the Dirac delta function. The parameter β controls the degree of homogeneity of each region in the image. It is assumed known a priori in this paper. However, it could be also included within the Bayesian model and estimated using the strategy described in [13].

2.3.2. Abundance matrix \mathbf{A}

A Dirichlet prior is assigned to the abundances to satisfy the physical PSTO constraints [14]. Each spatial class k is assigned a different Dirichlet parameter vector $\mathbf{c}_k = (c_{1k}, \dots, c_{Rk})^T$ as follows

$$\mathbf{a}_n | z_n = k, \mathbf{c}_k \sim \text{Dir}(\mathbf{c}_k), \text{ for } n \in \mathcal{I}_k \quad (4)$$

where $\text{Dir}(\cdot)$ denotes the Dirichlet distribution, and $n \in \mathcal{I}_k$ means that \mathbf{y}_n belongs to the k th class (which is also equivalent to $z_n = k$). This prior allows the data to be grouped into several distinct clusters inside the simplex [14]. Moreover, to simplify the sampling procedure, we propose to reparameterize \mathbf{a}_n by using the $(R - 1) \times 1$ vector \mathbf{t}_n introduced in [15]. This reparameterization expresses the

¹Note that the matrix $\boldsymbol{\Omega}$ depends on the noise and endmember variances.

physical PSTO constraints by only using nonnegativity constraint $\mathbf{t}_n \in [0, 1]^{R-1}$, which is easily handled by the sampling procedure (see [11, 15] for more details about this reparametrization). Note finally that assigning a Dirichlet prior for \mathbf{a}_n corresponds to a beta distribution prior (with parameters $\sum_{i=r+1}^R c_{ik}$ and c_{rk}) for the independent coefficients t_{rn} , $r \in \{1, \dots, R-1\}$ and that $f(\mathbf{t}_n | z_n = k, \mathbf{c}_k) = \prod_{r=1}^{R-1} f(t_{rn} | z_n = k, \mathbf{c}_k)$.

2.3.3. Endmember means

The endmember mean matrix \mathbf{M} contains reflectances that should satisfy the following constraints $0 < \mathbf{m}_{rl} < 1, \forall r \in \{1, \dots, R\}, \forall l \in \{1, \dots, L\}$ [11]. Therefore, we choose a truncated Gaussian prior for each endmember [7, 11] denoted as $\mathbf{m}_r \sim \mathcal{N}_{[0,1]^L}(\widehat{\mathbf{m}}_r, \epsilon^2 \mathbb{I}_L)$, where $\widehat{\mathbf{m}}_r$ denotes an estimated endmember (resulting from an endmember extraction algorithm such as VCA [16]) and ϵ^2 is a fixed variance term defining the confidence that we have on this estimated endmember $\widehat{\mathbf{m}}_r$.

2.3.4. Endmember variances

The absence of knowledge about the endmember variances can be considered by choosing a Jeffreys distribution for the parameters σ_{rl}^2 , i.e., $f(\Sigma_{:l}) \propto \prod_{r=1}^R \frac{1}{\sigma_{rl}^2} \mathbf{1}_{\mathbb{R}^+}(\sigma_{rl}^2)$, where we have assumed prior independence between the endmember variances.

2.3.5. Noise variance prior

The noise effect should be smaller than the effect of endmember variability. Thus, it is assigned the following sparse exponential prior $f(\psi_n^2 | \lambda) = \lambda \exp(-\lambda \psi_n^2) \mathbf{1}_{\mathbb{R}^+}(\psi_n^2)$, where λ is a large coefficient imposing sparsity for ψ_n ($\lambda = 10^7$ in our simulations). We furthermore assume prior independence between the random variables $\psi_n^2, \forall n \in \{1, \dots, N\}$.

2.3.6. Dirichlet parameters

The Dirichlet parameters \mathbf{c}_k are assigned conjugate priors as defined in [17]. The parameter of this prior have been chosen to ensure a non-informative prior (flat distribution) (see [18] for more details).

2.4. Posterior distribution

The parameters of the proposed Bayesian model are included in the vector $\boldsymbol{\theta} = \{\boldsymbol{\theta}_p, \boldsymbol{\theta}_h\}$ where $\boldsymbol{\theta}_p = \{\mathbf{A}, \mathbf{M}, \boldsymbol{\Sigma}, \boldsymbol{\Psi}\}$ (parameters) and $\boldsymbol{\theta}_h = \{\mathbf{C}, \mathbf{z}\}$ (hyperparameters), with $\mathbf{C} = [\mathbf{c}_1, \dots, \mathbf{c}_K]$ an $(R \times K)$ matrix containing the Dirichlet parameters.

The joint posterior distribution of the unknown parameter/hyperparameter vector $\boldsymbol{\theta}$ can be computed from the following hierarchical structure

$$f(\boldsymbol{\theta}_p, \boldsymbol{\theta}_h | \mathbf{Y}) \propto f(\mathbf{Y} | \boldsymbol{\theta}_p) f(\boldsymbol{\theta}_p | \boldsymbol{\theta}_h) f(\boldsymbol{\theta}_h) \quad (5)$$

where $f(\boldsymbol{\theta}_p, \boldsymbol{\theta}_h) = f(\boldsymbol{\theta}_p | \boldsymbol{\theta}_h) f(\boldsymbol{\theta}_h) = f(\mathbf{A} | \mathbf{C}, \mathbf{z}) f(\mathbf{M}) f(\boldsymbol{\Sigma}) f(\boldsymbol{\Psi}) f(\mathbf{C} | \mathbf{z}) f(\mathbf{z})$, where we have assumed prior independence between the parameters.

Unfortunately, it is difficult to obtain closed form expressions for the standard Bayesian estimators associated with (5). These estimators are therefore approximated using an MCMC approach that generates samples asymptotically distributed according to (5). This is achieved using a hybrid Gibbs sampler that sequentially samples the abundance matrix \mathbf{A} , the mean endmember matrix \mathbf{M} , the variance of endmembers $\boldsymbol{\Sigma}$, the labels \mathbf{z} , the noise variances $\boldsymbol{\Psi}$ and the Dirichlet parameters \mathbf{C} , according to their conditional distributions [19]. Due to the large number of parameters to be sampled and to the complexity of the conditional distributions, we use a CHMC algorithm which improves the mixing properties of the sampler [10]. The parameters are finally estimated using the MMSE estimator for $\{\mathbf{A}, \mathbf{M}, \boldsymbol{\Sigma}, \boldsymbol{\Psi}, \mathbf{C}\}$ and the MAP estimator for the labels \mathbf{z} . Note that more details about the sampling procedure are available in [18].

3. SIMULATION RESULTS ON SYNTHETIC DATA

This section considers a 50×50 synthetic image generated according to (2) with $R = 3$ endmember means (concretion concrete, green grass and micaceous loam) that have been extracted from the ENVI software library [20]. Each endmember has its own distribution whose variance changes from one spectral band to another. This image contains $K = 3$ classes whose label maps have been generated using the Potts-Markov prior with $\beta = 1.5$. The abundances of each class share the same Dirichlet parameters as previously explained. Note that the generated abundances have been truncated ($a_r < 0.9, \forall r$) to avoid the presence of pure pixels in the image. Finally, we have considered a noise variance equal to 10^{-7} . The proposed unsupervised GNCM-based algorithm, denoted by UsGNCM, has been run using $N_{\text{bi}} = 11000$ burn-in iterations and $N_{\text{MC}} = 12000$ iterations. Our algorithm is compared with state of the art algorithms: (i) VCA+FCLS: the endmembers are extracted from the whole image using VCA [16] and the abundances are estimated using the FCLS algorithm [21], (ii) UsLMM: the unsupervised Bayesian algorithm of [22] is used to jointly estimate the endmembers and abundances, (iii) AEB: this is the automated endmember bundles algorithm proposed in [23] (used with 10% image subset and the VCA algorithm), and (iv) UsNCM: the proposed unmixing strategy with $\psi_n = 0$ (i.e., the additive noise \mathbf{e}_n of (2) is removed). In this case, the resulting algorithm reduces to the NCM model.

Table 1 reports the quality of the estimated abundances and endmembers when considering the averaged root mean square error (aRMSE) and the averaged spectral angle mapper (aSAM) criteria [18]. This table shows bad performance for VCA+FCLS and AEB algorithms which is mainly due to the absence of pure pixels in the considered images. The UsLMM provides better results. However, it appears to be sensitive to the variation of endmember/noise variances with respect to the spectral band and to the spatial correlations be-

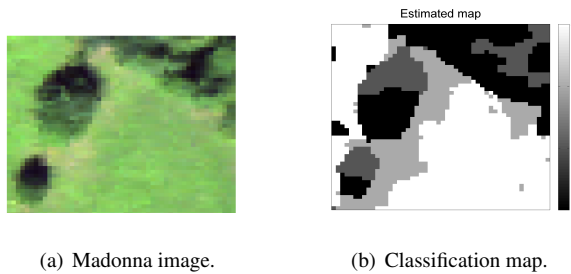
Table 1. Results on synthetic data.

	Criteria ($\times 10^{-2}$)		
	aRMSE (A)	aRMSE (M)	aSAM (M)
VCA+FCLS	3.71	2.68	6.74
UsLMM	0.76	0.49	0.94
AEB	9.46	4.20	8.72
UsNCM	0.56	0.19	0.43
UsGNCM	0.48	0.16	0.41

tween adjacent pixels. Indeed, the UsLMM does not consider spatial correlation between adjacent pixels of the image which limits its performance. Note also that the UsLMM algorithm provides one estimate for each endmember and does not take into account the spatial variability of endmembers in the processed image. The best performance is obtained by the proposed UsNCM and UsGNCM strategies that provide almost similar results. The slightly better performance of UsGNCM can be explained by the presence of the additive noise e_n . These results confirm the superiority of the proposed approach which accounts for SEV and spatial correlation between adjacent pixels and show its robustness to the absence of pure pixels in the image. Note finally that more results showing the interest of UsGNCM when increasing the number of endmembers and the image size are available in [18].

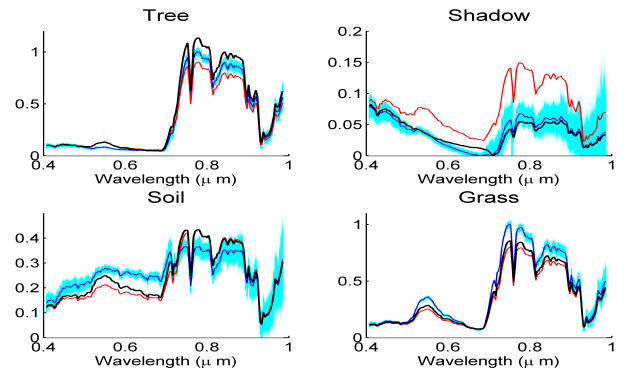
4. SIMULATION RESULTS ON REAL DATA

This section illustrates the performance of the proposed UsGNCM algorithm when applied to a real HS data set. The considered real image was acquired in 2010 by the Hypspec HS scanner over Villelongue, France. The dataset contains $L = 160$ spectral bands, 50×50 pixels and $R = 4$ components: tree, grass, soil and shadow (see Fig. 1 (left)).

**Fig. 1.** Real Madonna image and the estimated classification map using UsGNCM.

The estimated abundances using the UsGNCM algorithm are in good agreement with the FCLS and UsLMM results. These results are not presented here for brevity (see [18] for more details). In addition to unmixing, UsGNCM also provides a spatial classification of the considered scenes as shown in Fig. 1 (right). This classification clearly divides

the image into homogeneous areas characterized by different combinations of pure material (grass, tree,...). UsGNCM estimates both the mean and variance of each physical element in the scene which provides an SEV measure in the considered image. Fig. 2 shows the estimated endmember distributions as blue level areas for each endmember. These distributions are in good agreement with the point estimates obtained with VCA and UsLMM algorithms except for the shadow endmember. Indeed, VCA provides a different shadow endmember because it estimates the endmember as the purest pixel in the image while UsLMM and UsGNCM estimate both the abundances and endmembers resulting in a better shadow estimate (lower amplitude).

**Fig. 2.** The $R = 4$ endmembers estimated by VCA (continuous red lines), UsLMM (continuous black lines), UsGNCM (continuous blue lines) and the estimated endmember distribution (blue level areas) for the Madonna image.

5. CONCLUSIONS

This paper introduced a Bayesian model for unsupervised unmixing of HS images accounting for SEV. The proposed model was based on a generalization of the NCM defined by the endmembers of the scene, their variability controlled by a scale parameter (variance) and the abundances for each pixel of the scene. The observed image was also spatially classified into regions sharing homogeneous abundance characteristics. The physical constraints about the abundances were ensured by choosing a Dirichlet distribution for each spatial class of the image. Due to the complexity of the resulting joint posterior distribution, an MCMC procedure (based on a hybrid Gibbs sampler) was used to sample the posterior of interest and to approximate the Bayesian estimators of the unknown parameters using the generated samples. The proposed algorithm showed good performance for data presenting SEV and spatial correlation between adjacent pixels of the image. It was also shown to be robust to the absence of pure pixels in the observed scene. Future work includes the introduction of SEV in nonlinear mixing models. This point is an interesting issue that is currently under investigation.

6. REFERENCES

- [1] J.M. Bioucas-Dias, A. Plaza, N. Dobigeon, M. Parente, Qian Du, P. Gader, and J. Chanussot, "Hyperspectral unmixing overview: Geometrical, statistical, and sparse regression-based approaches," *IEEE J. Sel. Topics App. Earth Observations Remote Sens.*, vol. 5, no. 2, pp. 354–379, April 2012.
- [2] B. Somers, G. P. Asner, L. Tits, and P. Coppin, "Endmember variability in spectral mixture analysis: A review," *Remote Sensing of Environment*, vol. 115, no. 7, pp. 1603–1616, 2011.
- [3] A. Zare and K.C. Ho, "Endmember variability in hyperspectral analysis: Addressing spectral variability during spectral unmixing," *IEEE Signal Process. Mag.*, vol. 31, no. 1, pp. 95–104, Jan 2014.
- [4] A. Zare, P. Gader, D. Drashnikov, and T. Glenn, "Beta compositional model for hyperspectral unmixing," in *Proc. IEEE GRSS Workshop on Hyperspectral Image and Signal Processing: Evolution in Remote Sensing (WHISPERS)*, Gainesville, USA, Jun. 2013.
- [5] D. Stein, "Application of the normal compositional model to the analysis of hyperspectral imagery," in *Proc. IEEE Workshop Adv. Techniques for Analysis of Remotely Sensed Data*, Oct 2003, pp. 44–51.
- [6] O. Eches, N. Dobigeon, C. Mailhes, and J.-Y. Tourneret, "Bayesian estimation of linear mixtures using the normal compositional model. Application to hyperspectral imagery," *IEEE Trans. Image Process.*, vol. 19, no. 6, pp. 1403–1413, June 2010.
- [7] A. Zare, P. Gader, and G. Casella, "Sampling piecewise convex unmixing and endmember extraction," *IEEE Trans. Geosci. Remote Sens.*, vol. 51, no. 3, pp. 1655–1665, March 2013.
- [8] N. Bali and A. Mohammad-Djafari, "Bayesian approach with hidden markov modeling and mean field approximation for hyperspectral data analysis," *IEEE Trans. Image Process.*, vol. 17, no. 2, pp. 217–225, Feb. 2008.
- [9] O. Eches, N. Dobigeon, and J.-Y. Tourneret, "Enhancing hyperspectral image unmixing with spatial correlations," *IEEE Trans. Geosci. Remote Sens.*, vol. 49, no. 11, Nov 2011.
- [10] S. Brooks, A. Gelman, G. L. Jones, and X.-L. Meng, *Handbook of Markov chain Monte Carlo*, ser. Chapman & Hall/CRC Handbooks of Modern Statistical Methods. Taylor & Francis, 2011.
- [11] Y. Altmann, N. Dobigeon, S. McLaughlin, and J.-Y. Tourneret, "Unsupervised post-nonlinear unmixing of hyperspectral images using a Hamiltonian Monte Carlo algorithm," *IEEE Trans. Image Process.*, vol. 23, no. 6, pp. 2663–2675, June 2014.
- [12] Y. Altmann, N. Dobigeon, S. McLaughlin, and J.-Y. Tourneret, "Residual component analysis of hyperspectral images: Application to joint nonlinear unmixing and nonlinearity detection," *IEEE Trans. Image Process.*, vol. 23, no. 5, pp. 2148–2158, May 2014.
- [13] M. Pereyra, N. Dobigeon, H. Batatia, and J. Tourneret, "Estimating the granularity coefficient of a Potts-Markov random field within a Markov chain Monte Carlo algorithm," *IEEE Trans. Image Process.*, vol. 22, no. 6, pp. 2385–2397, June 2013.
- [14] J.M.P. Nascimento and J.M. Bioucas-Dias, "Hyperspectral unmixing based on mixtures of Dirichlet components," *IEEE Trans. Geosci. Remote Sens.*, vol. 50, no. 3, pp. 863–878, March 2012.
- [15] M. J. Betancourt, "Cruising the simplex: Hamiltonian Monte Carlo and the Dirichlet distribution," in *ArXiv e-prints*, Oct. 2013.
- [16] J. M. P. Nascimento and J. M. Bioucas-Dias, "Vertex component analysis: A fast algorithm to unmix hyperspectral data," *IEEE Trans. Geosci. Remote Sens.*, vol. 43, no. 4, pp. 898–910, April 2005.
- [17] Z. Ma, "Bayesian estimation of the Dirichlet distribution with expectation propagation," in *Proc. European Signal Process. Conf. (EUSIPCO)*, Bucharest, Romania, Aug. 2012.
- [18] A. Halimi, N. Dobigeon, and J.-Y. Tourneret, "Unsupervised unmixing of hyperspectral images accounting for endmember variability," in *ArXiv e-prints*, Jun. 2014.
- [19] C. P. Robert, *The Bayesian Choice: from Decision-Theoretic Motivations to Computational Implementation*, Springer Texts in Statistics. Springer-Verlag, New York, 2 edition, 2007.
- [20] RSI (Research Systems Inc.), *ENVI User's guide Version 4.0*, Boulder, CO 80301 USA, Sept. 2003.
- [21] D. C. Heinz and C. -I Chang, "Fully constrained least-squares linear spectral mixture analysis method for material quantification in hyperspectral imagery," *IEEE Trans. Geosci. Remote Sens.*, vol. 29, no. 3, pp. 529–545, March 2001.
- [22] N. Dobigeon, S. Moussaoui, M. Coulon, J.-Y. Tourneret, and A. O. Hero, "Joint Bayesian endmember extraction and linear unmixing for hyperspectral imagery," *IEEE Trans. Signal Process.*, vol. 57, no. 11, pp. 4355–4368, Nov. 2009.
- [23] B. Somers, M. Zortea, A. Plaza, and G.P. Asner, "Automated extraction of image-based endmember bundles for improved spectral unmixing," *IEEE J. Sel. Topics App. Earth Observations Remote Sens.*, vol. 5, no. 2, pp. 396–408, April 2012.